

Role of dysregulated ferroptosis-related genes in cardiomyocyte ischemia-reperfusion injury: Experimental verification and bioinformatics analysis

TIE HU^{1*}, WEN-PENG YU^{1*}, HUA-XI ZOU^{1*}, ZHI-HAO CHAI², SHU-YU LE², FA-JIA HU²,
YI-CHENG WANG², HUANG HUANG², SONG-QING LAI² and JI-CHUN LIU¹

¹Department of Cardiovascular Surgery, The Second Affiliated Hospital of Nanchang University;

²Institute of Cardiovascular Surgical Diseases, Jiangxi Academy of Clinical Medical Sciences, The First Affiliated Hospital of Nanchang University, Nanchang, Jiangxi 330006, P.R. China

Received May 10, 2023; Accepted August 9, 2023

DOI: 10.3892/etm.2023.12233

Abstract. Acute myocardial infarction is a life-threatening condition with high mortality and complication rates. Although myocardial reperfusion can preserve ischemic myocardial tissue, it frequently exacerbates tissue injury, a phenomenon known as ischemia-reperfusion injury (IRI). However, the underlying pathological mechanisms of IRI remain to be completely understood. Ferroptosis is a novel type of regulated cell death that is associated with various pathological conditions, including angiocardopathy. The purpose of this article was to elucidate the possible mechanistic role of ferroptosis in IRI through bioinformatics analysis and experimental validation. Healthy and IRI heart samples were screened for differentially expressed ferroptosis-related genes and functional enrichment analysis was performed to determine the potential crosstalk and pathways involved. A protein-protein interaction network was established for IRI, and 10 hub genes that regulate ferroptosis, including *HIF1A*, *EGFR*, *HMOX1*, and *ATF3* were identified. *In vitro*, an anoxia/reoxygenation (A/R) injury model was established using H9c2 cardiomyoblasts to validate the bioinformatics analysis results, and

extensive ferroptosis was detected. A total of 4 key hub genes and 3 key miRNAs were also validated. It was found that IRI was related to the aberrant infiltration of immune cells and the small-molecule drugs that may protect against IRI by preventing ferroptosis were identified. These results provide novel insights into the role of ferroptosis in IRI, which can help identify novel therapeutic targets.

Introduction

Cardiovascular diseases (CVDs) are life-threatening conditions with high mortality and complication rates despite the advances made in diagnostic and therapeutic approaches (1). The standard treatments for acute myocardial infarction (AMI) are reperfusion or reoxygenation, which limits the size of the infarct through percutaneous coronary intervention (PCI) or thrombolytic therapy (2). However, myocardial reperfusion or reoxygenation can cause further damage to the ischemic cardiac tissues, resulting in ischemia-reperfusion injury (IRI) (3,4). Several key pathological factors involved in IRI have been identified, including the excessive production of ROS, regulated cell death, Ca²⁺ overload, mitochondrial dysfunction, and inflammatory responses. However, the exact biological process and pathways related to IRI have not yet been elucidated (5). Thus, there is an urgent need to elucidate the pathological mechanisms underlying IRI to develop more effective pharmaceutical and other therapeutic strategies.

Ferroptosis is a novel type of programmed cell death initiated by iron-dependent lipid peroxidation, which leads to the condensation of mitochondrial membranes, and the reduction of mitochondrial cristae (6). It is a complex event mediated by multiple pathways and has been increasingly implicated in CVD (7). A previous study showed that the administration of deferoxamine during the reperfusion of isolated rabbit hearts significantly decreased the free radical content and protected heart tissue from IRI (8). Deferoxamine also reduced cardiac function injury after coronary artery bypass grafting (9). Dysregulated iron homeostasis is a leading cause of IRI, which increases the generation of hydroxyl radicals (•OH) via the Fenton reaction, thereby triggering ferroptosis, pyroptosis,

Correspondence to: Professor Ji-Chun Liu, Department of Cardiovascular Surgery, The Second Affiliated Hospital of Nanchang University, 1 Minde Road, Nanchang, Jiangxi 330006, P.R. China

E-mail: liujichun999@yeah.net

Dr Song-Qing Lai, Institute of Cardiovascular Surgical Diseases, Jiangxi Academy of Clinical Medical Sciences, The First Affiliated Hospital of Nanchang University, 17 Yongwai Road, Nanchang, Jiangxi 330006, P.R. China

E-mail: ndyfy03743@ncu.edu.cn

*Contributed equally

Key words: ischemia-reperfusion injury, ferroptosis, anoxia/reoxygenation, database, hub genes

necroptosis, and other forms of programmed cell death (10). Although these studies established the pathological role of ferroptosis in IRI, the underlying mechanism and targets remain unclear (11).

The aim of the present study was to elucidate the role of ferroptosis in the pathophysiology of IRI through bioinformatics analysis and *in vitro* experiments. The association between ferroptosis and IRI was confirmed and the differentially expressed genes related to ferroptosis were identified.

Materials and methods

Data collection. Gene expression datasets associated with myocardial reperfusion injury were downloaded from GEO (<https://www.ncbi.nlm.nih.gov/geo/>) (12) using ‘ischemia-reperfusion’, ‘post-ischemia’, and ‘after ischemia’ as the key words. The inclusion criteria for the microarray datasets were: i) Consisted of cardiac tissue specimens, ii) included control and ischemia/reperfusion samples, and iii) had an adequate sample size (both IRI and normal samples >3). Accordingly, four microarray datasets were obtained from GEO. The first two datasets were GSE58486 (3 control and 6 IRI heart samples) and GSE160516 (4 control and 12 IRI heart samples), which were screened for differentially expressed genes (DEGs) between the normal and IRI heart samples, as well as for hub genes. GSE4105 (6 control and 6 IRI heart samples) was used for hub gene validation. GSE124176 (3 control and 3 IRI heart samples) was used for screening differentially expressed miRNAs (DEmiRs) between the normal and IRI heart samples. Ferroptosis-related genes (FRGs) were downloaded from FerrDb (<https://www.zhounan.org/ferrdb>) (13).

Identification of DEGs, differentially expressed ferroptosis-related genes (DEFRGs), and DEmiRs. The genes were first converted to the official gene IDs based on the annotations from the corresponding platform. The gene expression values were then transformed to a log₂ format and quantile normalization was performed. Identifying and extracting DEGs using the limma package (version 3.48.0) (14) in R software (version 3.6.3) (15), with $|\log_2FC| \geq 1$ and P-values <0.05 as the thresholds for selection (where FC is fold change). After removing repetitive genes, 388 genes were included in the FRG set (Table SI). In addition, 51 DEFREGs were obtained using the VennDiagram package (version 1.7.3) (16) in R, and 8 DEmiRs were identified in GSE124176.

Gene set enrichment analysis (GSEA). GSEA was conducted on the 388 FRGs to evaluate the functional correlation between ferroptosis and myocardial reperfusion injury. Briefly, the FRGs in GSE58486 and GSE160516 were scored and ranked based on expression values to evaluate the enrichment score (ES) and core genes. FRGs with a false discovery rate (FDR) <0.25 and a P-value <0.05 were considered significantly enriched.

Functional and pathway enrichment analyses of DEFREGs. DEFREGs between the normal and IRI heart samples were submitted to Data for Annotation, Visualization, and Integrated Discovery (DAVID; david.ncifcrf.gov/) (17,18) for Gene Ontology (GO) (19,20) and Kyoto Encyclopedia of Genes

and Genomes (KEGG) enrichment analyses (21). P<0.05 was considered to indicate a statistically significant difference.

Construction of a protein-protein interaction (PPI) network and hub gene identification. A PPI network of the DEFREGs was constructed using the STRING database (<https://string-db.org/>) (22) and visualized in Cytoscape software (version 3.8.2) (23). The hub genes in DEFREGs were identified by Cytohubba, a Cytoscape plugin based on the MCC algorithm (24). Each DEFREG in the PPI network was allocated a value, and the genes were ranked accordingly. The top 10 genes were screened as hub genes.

Verification of hub genes in GSE4105. The expression levels of the hub genes were validated in the GSE4105 dataset. Comparisons between the control and IRI samples were made using a Student's t-test and P<0.05 was considered to indicate a statistically significant difference.

Prediction of target genes and transcription factors of DEmiRs. The target mRNAs of the DEmiRs extracted from GSE124176 were predicted using TargetScan (targetscan.org/), miRwalk (<http://mirwalk.umm.uni-heidelberg.de/>), and miRDB (<http://www.mirdb.org/>) (25-27). After removing the duplicate genes, the overlapping differentially expressed target genes and DEFREGs were extracted using the VennDiagram package in R. Potential transcription factors (TFs) for key DEmiRs were screened using the TransmiR v2.0 database (<http://www.cuilab.cn/transmir>) (28). The overlapping potential TFs and DEFREGs were considered the key TFs involved in the miRNA-mRNA-TF network.

Construction of the DEmiR-target gene-TF regulatory network. A TF-miRNA-mRNA regulatory network was established based on the key TFs, key DEmiRs, and target genes and visualized using Cytoscape to identify the regulatory pathways.

H9c2 cell culture and treatment. Rat H9c2 cardiomyocytes, purchased from the Cell Bank/Stem Cell Bank (Chinese Academy of Sciences, China) were cultured in high-glucose DMEM (H-DMEM) (HyClone, Cytiva) containing 10% FBS (Gibco, Thermo Fisher Scientific, Inc.), 100 U/ml penicillin and 100 µg/ml streptomycin (Beijing Solarbio Science & Technology Co., Ltd.) at 37°C under in a humidified incubator supplied with 5% CO₂ air and 21% O₂. For the experiments, the cells were treated with ferrostatin-1 (Fer-1, MedChemExpress) freshly prepared in DMSO.

Establishment of the *in vitro* IRI model. The cellular IRI model was established as described previously (29). Briefly, H9c2 cells were subjected to anoxia for 3 h in a specialized medium (1 mM CaCl₂, 10 mM KCl, 20 mM HEPES, 98.5 mM NaCl, 1.2 mM MgSO₄, 6 mM NaHCO₃, 0.9 mM NaH₂PO₄, and 40 mM sodium lactate, pH 6.8) in a humidified incubator supplied with 95% N₂ and 5% CO₂, and then reoxygenated for 2 h in a reoxygenation medium (1 mM CaCl₂, 5.5 mM glucose, 5 mM KCl, 20 mM HEPES, 129.5 mM NaCl, 1.2 mM MgSO₄, 20 mM NaHCO₃, and 0.9 mM NaH₂PO₄, pH 7.4) in a humidified incubator supplied with 95% O₂ and 5% CO₂. The cells were

treated with 5 mM Fer-1 for 2 h prior to anoxia/reoxygenation (A/R) to inhibit ferroptosis.

Measurement of cell viability. H9c2 cells were seeded in 96-well plates at a density of 1×10^4 cells per well in 100 μ l H-DMEM and cultured for 24 h. Following treatment, cell viability was determined using a Cell Counting Kit-8 assay (GlpBio Technology; cat. no. #GK10001) and absorbance at 450 nm was assessed using a Multiskan FC microplate reader (Thermo Fisher Scientific, Inc.).

Measurement of total iron concentration and malondialdehyde (MDA) levels. Treated H9c2 cells were harvested, sonicated, and centrifuged at 12,000 g for 10 or 5 min at 4°C to remove cell debris. The quantity of MDA and iron in the supernatants were analyzed using specific assay kits (Beyotime Institute of Biotechnology, cat. no. #S01031M; Pulilai Gene Technology, cat. no. #E1042), and the absorbance was measured at 530 and 560 nm, respectively, using a Multiskan FC microplate reader.

Measurement of intracellular ROS generation. Intracellular ROS generation was detected using an ROS assay kit (Beyotime Institute of Biotechnology, cat. no. #S0033M). Briefly, H9c2 cells were cultured with 10 μ M DCFH-DA solution in H-DMEM for 20 min at 37°C in the dark and washed once with H-DMEM. DCFH-DA fluorescence was detected using a fluorescence Olympus IX73 microscope (Olympus Corporation) at an excitation wavelength of 488 nm and an emission wavelength of 525 nm.

Transmission electron microscopy (TEM). Following the different treatments, H9c2 cells were rapidly gathered and incubated in 2% glutaraldehyde for 2 h. Then, the cells were observed by transmission electron microscopy after washing, dehydration, embedding in Epon 812, sectioning (60 nm), and stained with 2% uranyl acetate and 2.6% lead citrate for 8 min at 37°C. Finally, the Flameng scoring method was used to assess the ultrastructural injury of the mitochondria (30).

Measurement of intracellular lipid ROS. Following the different treatments, H9c2 cells were collected and incubated with 10 μ M C11-BODIPY581/591 (GlpBio) in the dark for 1 h at 37°C and washed twice with PBS. The cells were centrifuged at 400 g for 5 min at 25°C and resuspended in PBS supplemented with 10% FBS. The levels of lipid ROS were measured using a Cytomics FC500 flow cytometer (Beckman Coulter, Inc.). Increases in lipid ROS shifted the fluorescence emission peak from ~590 to ~510 nm, which reflected increased lipid ROS levels. The flow cytometry data were analyzed using NovoExpress (v.6.2; Agilent Technologies, Inc.).

Western blot analysis. Western blotting was performed as described in our previous study (21). Cardiomyocytes were lysed in RIPA lysis buffer (Beyotime Institute of Biotechnology) containing 1% PMSF, and the protein concentration was measured using the BCA protein assay kit (GLPBIO). 30 μ g/lane from each sample were loaded on a 10% SDS-gel, resolved by SDS-PAGE, and then transferred to PVDF membranes. After blocking with 5% non-fat dry milk in TBS with 0.1% Tween 20 (TBST) at room temperature

for 2.5 h, the membranes were incubated overnight with anti-PTGS2 (ProteinTech Group, Inc.; cat. no. #12375-1-AP; 1:1,000), anti-GPX4 (ZENBIO; cat. no. #381958; 1:1,000), and anti- β -actin (OriGene Technologies, Inc.; cat. no. #TA-09; 1:1,000) antibodies at 4°C. The membranes were then washed three times and incubated with the secondary antibody (Beyotime Institute of Biotechnology; cat. no. #A0208; 1:3,000) for 1.5 h at room temperature. The protein bands were detected using an ultra-high-sensitivity ECL kit (Beyotime Institute of Biotechnology) and imaged using FluorChem FC3 (ProteinSimple). The signal intensities of the bands were quantified using ImageJ 1.8.0 (National Institutes of Health) and normalized to that of the respective β -actin band.

Reverse transcription-quantitative (RT-q)PCR. RT-qPCR was performed as described previously (19). Briefly, total RNA, including miRNA, was isolated from H9c2 cells using TRIzol[®] reagent (Invitrogen; Thermo Fisher Scientific, Inc.) and reverse-transcribed to cDNA using RevertAid[™] (Thermo Fisher Scientific, Inc.) after evaluating the quality and concentration of RNA. RT were as follows: 42°C for 1 h, 72°C for 10 min. qPCR was performed using Power SYBR Green PCR MasterMix (Thermo Fisher Scientific, Inc.) on an Applied Biosystems StepOnePlus Real-time PCR system (Thermo Fisher Scientific, Inc.). The RT-PCR process involved initial denaturation at 95°C for 10 min, followed by thermocycling 95°C for 15 sec, and 60°C for 1 min, repeated 40 cycles. Relative mRNA expression levels were calculated using the $2^{-\Delta\Delta Cq}$ method (31). All primers were synthesized by Sangon Biotech Co., Ltd.; the sequences of the primers used in the present study are shown in Table SII.

Immune infiltration analysis. The expression data of GSE58486 and GSE160516 were uploaded to Immune Cell Abundance Identifier (<http://bioinfo.life.hust.edu.cn/web/ImmuCellAI/>) (32) to evaluate the infiltration ratio of different immune cells. The infiltration ratio of 36 types of immune cells was calculated using the ImmuCellAI algorithm and compared between control and IRI samples using Student's t-test. $P < 0.05$ was considered to indicate a statistically significant difference.

Prediction of potential therapeutic drugs. The DSigDB database (<http://tanlab.ucdenver.edu/DSigDB>) was used to predict potential therapeutic drugs for IRI, with an FDR of < 0.05 and a combined score of $> 2,000,000$ as the cutoff criteria (33).

Statistical analysis. Data are presented as the mean \pm standard derivation. Statistical analysis was performed using GraphPad Prism 8.0 (GraphPad Software, Inc.) or the Sangerbox platform. An unpaired two-tailed Student's t-test was used to compare differences between two groups and a one-way ANOVA followed by a Dunnett's post hoc multiple comparisons test was used to compare differences between ≥ 3 groups. $P < 0.05$ was considered to indicate a statistically significant difference.

Results

Study protocol. The overall workflow of this study is shown in Fig. 1.

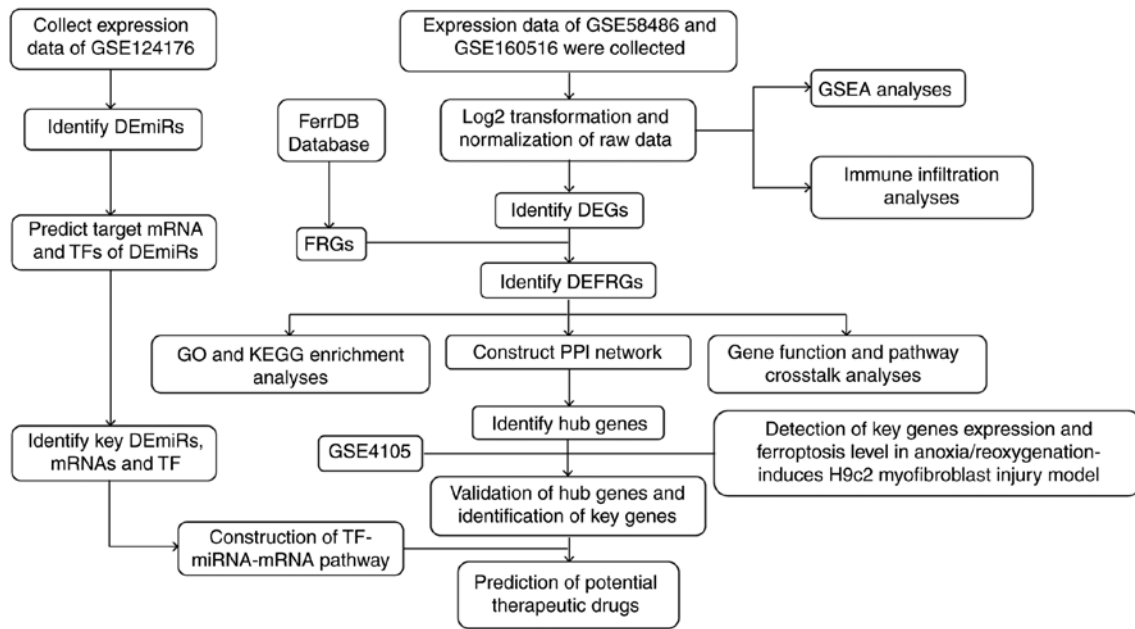


Figure 1. Overall workflow of the present study. DEG, differentially expressed gene; miRNA, microRNA; DE miRNA, differentially expressed miRNA; TF, transcription factor; FRG, ferroptosis related gene; DEFRG, differentially expressed FRG; GO, Gene Ontology; KEGG, Kyoto Encyclopedia of Genes and Genomes; PPI, protein-protein interaction; GSEA, gene set enrichment analysis.

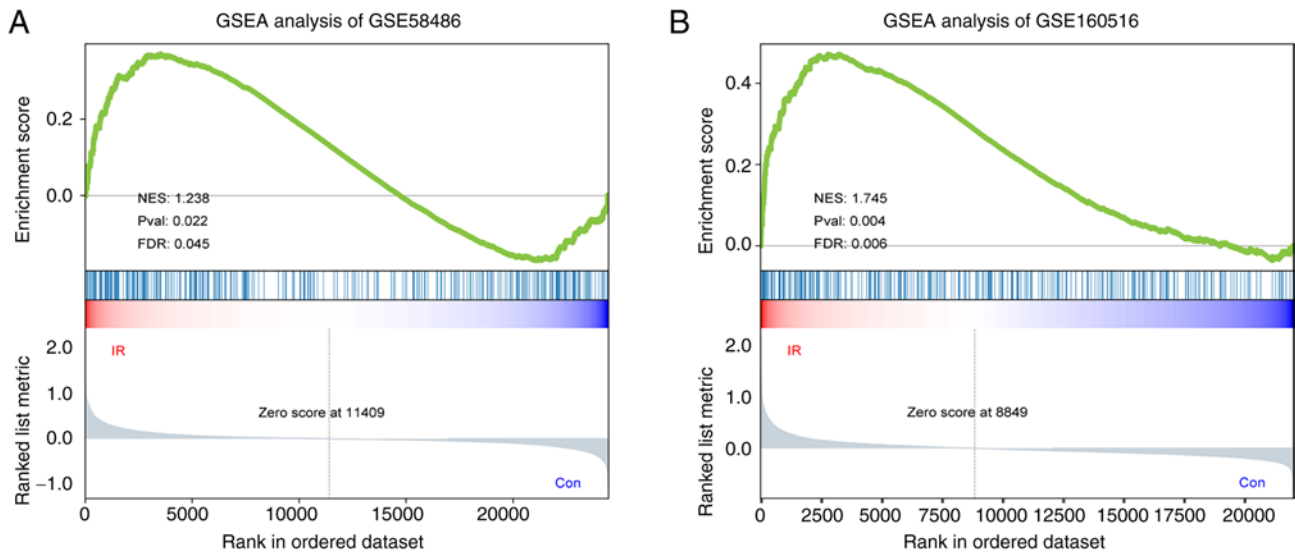


Figure 2. GSEA. GSEA of the FRG set in (A) GSE58486 and (B) GSE160516. GSEA, gene set enrichment analysis; FRG, ferroptosis related gene; NES, normalized enrichment score; FDR, false discovery rate.

Relationship between ferroptosis and myocardial reperfusion. GSEA of the FRG dataset was used to determine whether ferroptosis was a key pathophysiological factor in IRI. The genes associated with ferroptosis were significantly enriched in the GSE58486 and GSE160516 IRI samples with a normalized enrichment score (NES) of >1 (nominal P-value <0.05 and FDR <0.25 ; Fig. 2A and B), suggesting a relationship between IRI and ferroptosis. A total of 87 and 84 genes were extracted from GSE58486 and GSE160516, respectively, for GSEA and are listed in Table SIII.

Screening of DEGs, DE miRNAs, and DEFRGs. A total of 1,287 DEGs (673 upregulated and 614 downregulated) in GSE58486

and 1,079 DEGs (752 upregulated and 327 downregulated) in GSE160516 were screened (Fig. 3A and B). A total of eight DE miRNAs (4 downregulated and 4 upregulated) were obtained from GSE124176 (Table I). Additionally, 51 DEFRGs were identified based on the overlapping genes between the 388 FRGs downloaded from FerrDb, and the DEGs screened from GSE58486 and GSE160516 (Fig. 3E, Table SIV). The DEFRGs showed distinct expression patterns in the normal and IRI samples (Fig. 3C and D).

Functional and pathway enrichment analysis of DEFRGs. The DEFRGs were functionally annotated by GO enrichment and KEGG pathway analyses. The GO terms were categorized into

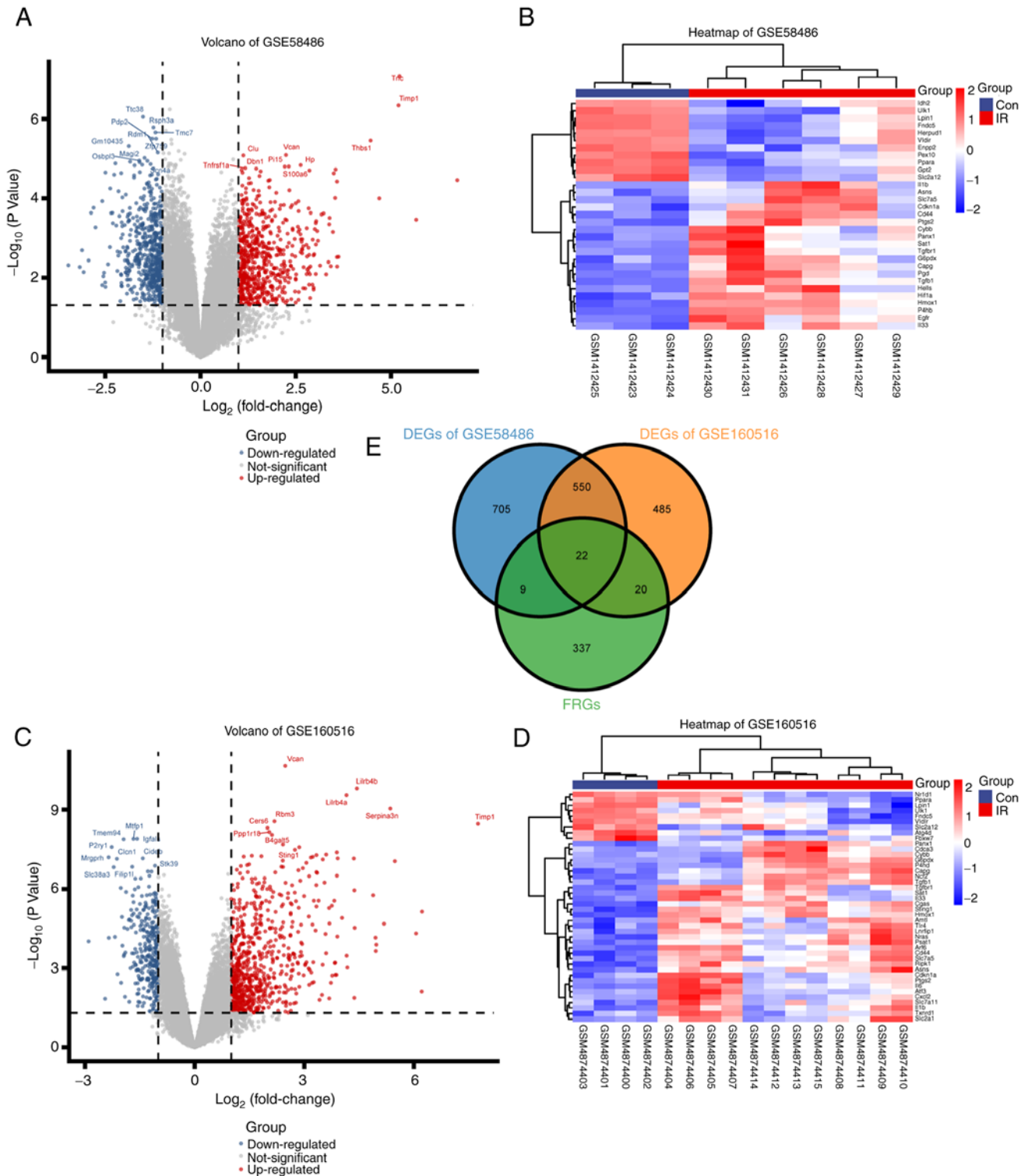


Figure 3. Identification of the DEFRGs. (A) Volcano plot of DEFRGs in GSE58486. (B) Heatmap of the DEFRGs in GSE160516. (C) Volcano plot of the DEFRGs in GSE58486. (D) Heatmap of the DEFRGs in GSE160516. (E) Venn diagram of the DEGs between DEGs in GSE58486 and GSE160516 and FRGs in the FerrDb database. DEG, differentially expressed gene; FRG, ferroptosis related gene; DEFRG, differentially expressed FRG.

biological process (BP), cellular component (CC), and molecular function (MF). The DEFRGs were significantly enriched in BP terms such as inflammatory response, positive regulation of the apoptotic process, and positive regulation of transcription from RNA polymerase II promoter (Fig. 4A). Cytoplasm, membrane, and cytosol were significantly enriched CC terms (Fig. 4B), and those related to the MF category were identical protein binding,

protein binding, and macromolecular complex binding (Fig. 4C). The pathways significantly associated with DEFRGs included the hypoxia-inducible factor (HIF)-1, ferroptosis, and NF- κ B signaling pathways (Fig. 4D). The interactions between DEFRGs and the above functions and pathways were explored and found that the regulation of DEFRGs during myocardial reperfusion injury may involve multiple genes and pathways (Fig. 5).

Table I. Key differentially expressed miRs obtained from GSE124176.

| miRNA_ID | logFC | P-value |
|-----------------|--------------|--------------------------|
| mmu-miR-23b-5p | -1.059027778 | 0.000560393 ^c |
| mmu-miR-1940 | 1.042500000 | 0.001688678 ^b |
| mmu-miR-7030-5p | 1.022222222 | 0.001989443 ^b |
| mmu-miR-706 | -1.084861111 | 0.005639392 ^b |
| mmu-miR-582-5p | 2.275000000 | 0.009632056 ^b |
| mmu-let-7f-1-3p | -1.036805556 | 0.01466152 ^a |
| mmu-miR-714 | -1.053055556 | 0.02414709 ^a |
| mmu-miR-466j | 1.441666667 | 0.049095123 ^a |

^aP<0.05, ^bP<0.01, ^cP<0.001. miR/miRNA, microRNA.

Construction of a PPI network and extraction of hub genes. To further understand the interactions between these DEFRGs, a PPI network was constructed using the STRING database (Fig. 6A). The hub genes were extracted using the Cytohubba plugin of Cytoscape and included IL-1B, HIF-1A, IL-6, epidermal growth factor receptor (EGFR), toll-like receptor (TLR)4, transforming growth factor (TGF)-B1, heme oxygenase (HMOX)1, prostaglandin-endoperoxide synthase (PTGS)2, activating transcription factor (ATF)3, and peroxisome proliferator-activated receptor α (PPAR α). The interactions between the DEFRGs and hub genes are shown in Fig. 6B and D. The differential expression of hub genes between normal and IRI hearts is shown in Fig. 6C.

Verification of hub gene expression in GSE4105. The differential expression of hub genes in the GSE4105 dataset was analyzed to further clarify their role in IRI. HIF-1A, EGFR, TGF-B1, HMOX1, and ATF3 showed similar expression patterns in GSE4105 (Fig. 7) and were markedly upregulated in the IRI samples compared to the controls. Thus, these 5 genes were considered key FRGs involved in myocardial reperfusion injury.

Ferroptosis is induced in cardiomyocytes subjected to A/R injury *in vitro*. To validate the results of the bioinformatics analysis, an A/R injury model was established to simulate IRI *in vitro* and ferroptosis induction was explored. The viability of H9c2 cells subjected to A/R was markedly decreased compared to that of cells cultured under normoxic conditions. Interestingly, pretreatment with the ferroptosis inhibitor Fer-1 protected the cells against A/R injury (Fig. 8A). The levels of PTGS2 and GPX4 proteins were also analyzed, as established markers of ferroptosis (34,35), in the treated H9c2 cells. A/R treatment increased the expression of PTGS2 and decreased that of GPX4, whereas Fer-1 neutralized the effect of A/R and restored the levels of both proteins (Fig. 8B and C). Furthermore, cells subjected to A/R showed a significant increase in the cytoplasmic levels of total iron and MDA compared to the controls, which was attenuated by Fer-1 pretreatment (Fig. 8E and F). In addition, Fer-1 pretreatment alleviated A/R-induced increases in ROS levels (Fig. 8D). Previous studies showed that lipid peroxidation and extensive

mitochondrial injury are key signs of ferroptosis (34). The mitochondria in A/R-induced H9c2 cells were significantly distorted, and the Flameng scores were significantly increased; Fer-1 pretreatment protected against such pathological changes (Fig. 8G and H). As shown in Fig. 8I and J, the content of lipid ROS in the A/R group was significantly increased compared to the control group, and Fer-1 pretreatment abolished the effects induced by A/R treatment. These findings suggested significant activation of the ferroptosis program in cardiomyocytes in response to A/R injury. The expression levels of HIF-1A, EGFR, TGF-B1, HMOX1, and ATF3, the five key FRGs identified in bioinformatics analysis, were analyzed in the treated cells. HIF-1A, EGFR, HMOX1, and ATF3 mRNA levels increased significantly after A/R treatment and were downregulated by Fer-1, indicating that these genes are key regulators of ferroptosis during IRI (Fig. 8K-O).

Immune infiltration analysis. Previous studies showed that ferroptosis is a form of immune cell death (36,37). Therefore, the abundance of 36 immune cell types between IRI and control samples was compared using the ImmuCellAI algorithm. Consistent with the clustered heatmap results, immune infiltration was significantly different between the IRI and control samples in the GSE58486 dataset, whereas the differences were not obvious in the GSE160516 dataset (Fig. 9A and C). However, the infiltration of M1 and M2 macrophages was markedly increased in the IRI samples in both datasets.

Single Sample Gene Set Enrichment Analysis (ssGSEA) results showed that the abundance of NK and CD4 T cells, eosinophils, CD4 Tm cells, and Tregs was notably lower in the IRI samples in both the GSE58486 and GSE160516 datasets (Fig. 9B and D). In addition, the IRI and control sample infiltration scores evaluated by ssGSEA were significantly different in GSE58486 (P<0.05) and GSE160516 (P<0.05).

Prediction of the target genes and TFs of DEmiRs. The target genes of DEmiRs were predicted using miRwalk, TargetScan, and miRDB; 248 upregulated and 306 downregulated mRNAs that were common to all three databases were screened. Two upregulated and one downregulated target mRNA overlapped with the DEFRG set (Fig. 10A and C). Three DEmiRs, including mmu-let-7f-3p, mmu-mir-706, and mmu-mir-466j, were the putative regulators of these overlapping genes and, thus, were considered key miRNAs involved in ferroptosis during myocardial reperfusion injury. The target TFs of these key DEmiRs were then screened in the TransmiR database, and ATF3 was identified as the key TF for the DEFRGs (Fig. 10B and D).

Establishment of TF-miRNA-mRNA network. To further elucidate the role of key miRNAs in IRI, the expression of mmu-let-7f-3p, mmu-mir-706, and mmu-mir-466j was assessed *in vitro*. As shown in Fig. 10E, mmu-mir-466j miRNA levels were significantly increased in the A/R group compared to the control group and downregulated by Fer-1 pretreatment. The levels of mmu-let-7f-3p and mmu-mir-706 miRNA were significantly reduced in the A/R group, whereas Fer-1 pretreatment increased mmu-let-7f-3p and mmu-mir-706 levels compared with the A/R group (Fig. 10F and G). A TF-miRNA-mRNA network was also constructed. As shown

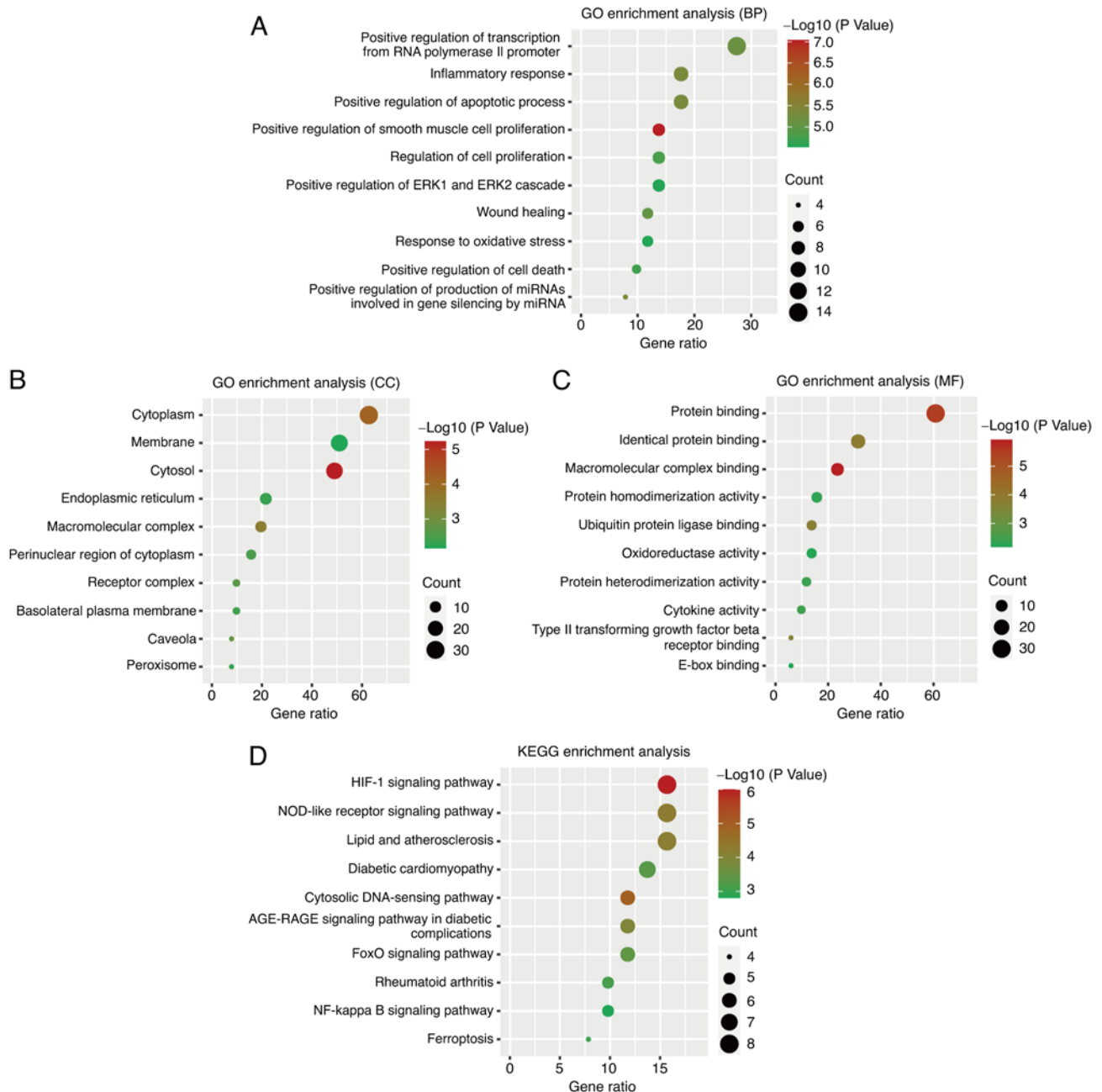


Figure 4. GO and KEGG enrichment analyses of the DEFRGs. GO enrichment analyses of DEFRGs in (A) the BP category, (B) CC category, and (C) the MF category. (D) KEGG enrichment analysis of the DEFRGs. DEFRG, differentially expressed ferroptosis-related genes; GO, Gene Ontology; KEGG, Kyoto Encyclopedia of Genes and Genomes; BP, biological process; CC, cellular component; MF, molecular function.

in Fig. 10H, the network consisted of three key DEmiRs, three target genes, and one TF.

Targeted drug prediction of hub genes. The DSigDB database was used to predict drugs correlated with the hub genes, which can be potentially effective against IRI. The candidate drugs were screened based on adjusted P-values and combined scores. The top 10 predicted target drugs ranked by combined scores are listed in Fig. 11A. As shown in Fig. 10E, the top three drugs significantly correlated with the target genes (adjusted P-value < 0.0001, combined score > 2x10⁶) were resveratrol (Fig. 11B, combined score=4,650,762), quercetin (Fig. 11C, combined score=3,110,735), and retinoic acid (Fig. 11D, combined score=2,436,510).

Discussion

Ferroptosis, a novel type of programmed cell death characterized by iron-induced lipid membrane peroxidation, is a pathological factor in several types of cardiovascular diseases, including heart failure, and acute aortic dissection (38-40). However, the association between ferroptosis and IRI remains unclear. Ischemic heart disease is often succeeded by myocardial IRI, which is the result of the excessive production of free radicals and cardiomyocyte apoptosis due to mitochondrial dysfunction, calcium overload, and increased heat shock protein levels (41). Several clinical studies showed that iron overload was a critical factor involved in incomplete left ventricular remodeling after IRI (42). Likewise, the inhibition of glutaminolysis alleviated

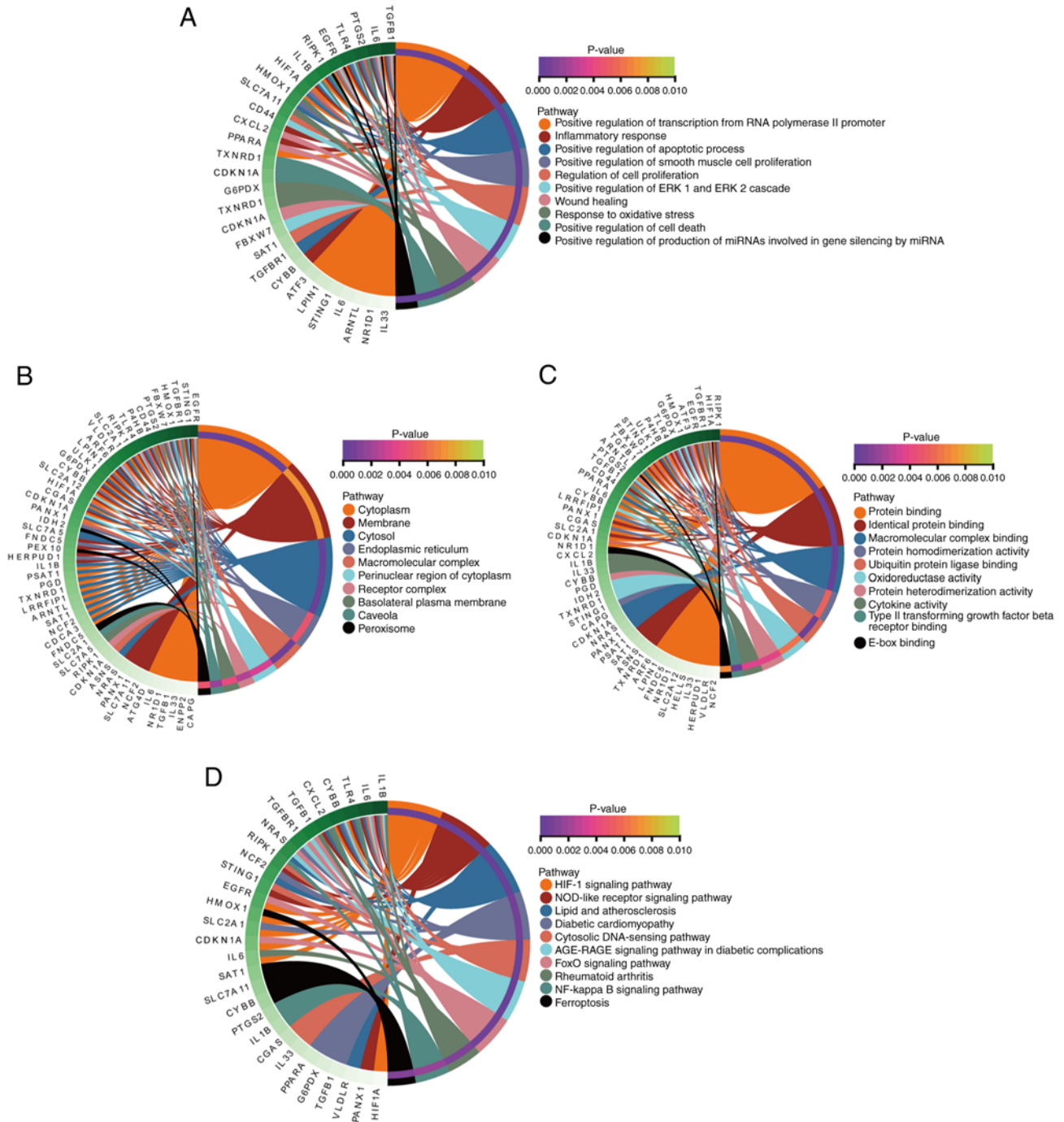


Figure 5. Crosstalk analysis between the DEFRGs and (A) gene functions in BP, (B) gene functions in CC, (C) gene functions in MF, and (D) KEGG pathways. D DEFRG, differentially expressed ferroptosis related genes; GO, Gene Ontology; KEGG, Kyoto Encyclopedia of Genes and Genomes; BP, biological process; CC, cellular component; MF, molecular function.

IRI by blocking ferroptosis (43). Based on these reports, it is hypothesized that ferroptosis plays a significant role in the development of IRI. Here, Fer-1 pretreatment could remarkably reduce excess lipid ROS generation, iron accumulation, and excessive mitochondrial injury induced by A/R treatment. Based on the primary manifestations of ferroptosis, it was confirmed that ferroptosis was involved in the pathological process of IRI. To this end, the genes related to ferroptosis were screened and their regulatory networks in IRI were explored through bioinformatics analysis using multiple transcriptomic datasets of normal and ischemic heart tissue.

Consistent with previous studies, several FRGs were aberrantly expressed in the IRI samples, indicating that the activation of ferroptosis is a key pathological factor (44). In addition, DEFRGs were significantly enriched in GO terms related to ferroptosis and oxidative stress, which is a major trigger of ferroptosis, apoptosis, and the inflammatory response (45). Other GO terms associated with DEFRGs included identical protein binding and macromolecular complex binding, which may also affect the pathological process of IRI. KEGG analysis revealed that the HIF-1 signaling pathway and NOD-like receptor signaling pathway

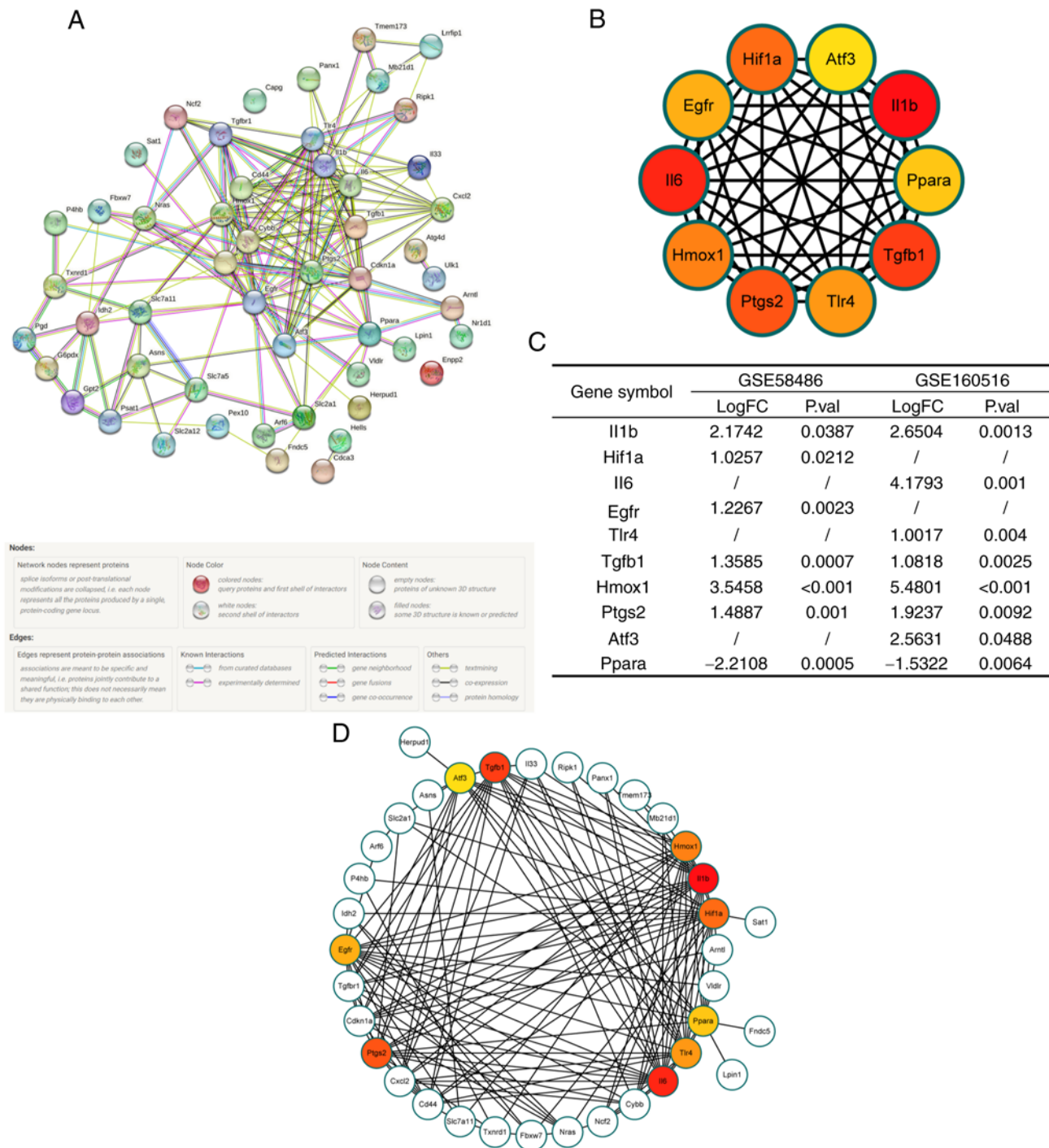


Figure 6. PPI network construction and identification of the hub genes. (A) PPI network of all the DEFERGs; genes with no connected dots are hidden. (B) Crosstalk between the top 10 hub genes ranked using the MCC algorithm; the deeper the color of the dot, the more advanced the rank order of the hub gene was. (C) Differential expression of hub genes in the IRI samples from GSE58486 and GSE160516; (D) Crosstalk between top 10 hub genes ranked by MCC algorithm and other DEFERGs. DEFRG, differentially expressed ferroptosis related gene; PPI, protein-protein interaction; IRI, ischemia-reperfusion injury.

may mediate ferroptosis during IRI, although neither pathway has yet been implicated in IRI.

To further clarify the mechanisms underlying ferroptosis activation in IRI, a PPI network of DEFERGs was constructed, and several hub genes were identified, of which *HIF1A*, *EGFR*, *HMOX1*, and *ATF3* were validated experimentally in an *in vitro* A/R model. Previous studies showed that these critical genes participate in the regulation of ferroptosis (46-49). Furthermore, the *HIF1A/PTGS2* pathway

aggravates ferroptosis and mediates myocardial injury and inflammation after coronary microembolization (50). By contrast, the overexpression of *ATF3* prevents the activation of ferroptosis by erastin and RSL3 in cardiomyocytes (51). There are currently no reports on the role of *EGFR* and *HMOX1* in cardiovascular diseases in the context of ferroptosis to the best of our knowledge. Since the aforementioned genes also participate in other pathological processes, they may regulate IRI through mechanisms independent of ferroptosis. Thus, it is

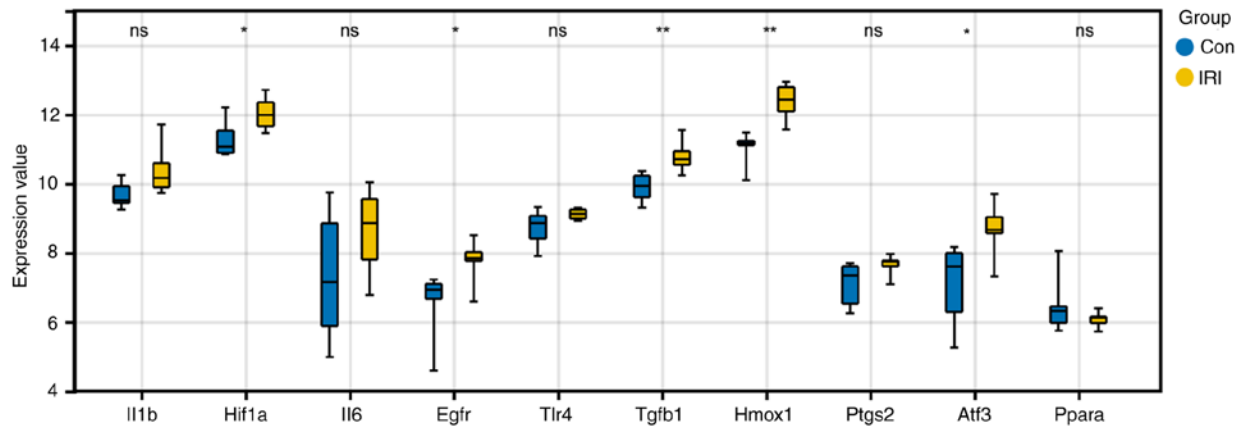


Figure 7. Expression levels of hub genes in IRI and normal heart samples in the GSE4105 dataset. * $P<0.05$, ** $P<0.01$. ns, not significant; IRI, ischemia-reperfusion injury.

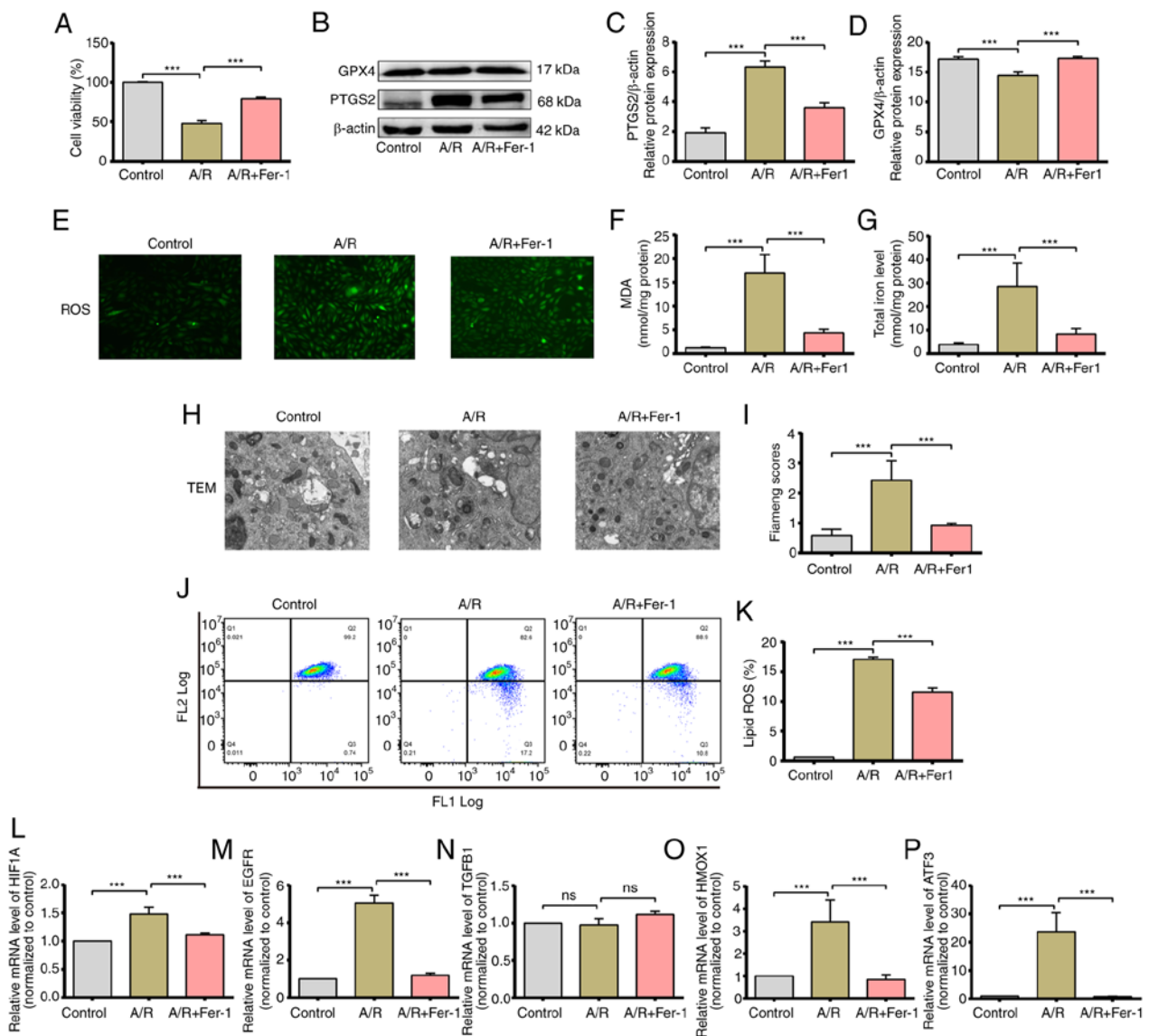


Figure 8. Activated ferroptosis and validation of the expression of hub genes in the H9c2 A/R model, H9c2 myofibroblasts were exposed to anoxic conditions for 3 h and then reoxygenated for 2 h in the after pretreatment with 5 mM Fer-1. (A) Cell viability was measured using a CCK-8 assay. (B and C) Protein expression levels of PTGS2 and GPX4. (D) Representative fluorescence images of ROS in H9c2 myofibroblasts. (E) MDA levels and (F) total iron levels in H9c2 myofibroblasts. (G and H) TEM images and the Flameng scores of H9c2 cells. magnification, $\times 8,000$; scale bar, $2 \mu\text{m}$. (I and J) Lipid ROS levels of were assessed using C11-BODIPY staining. (K-P) mRNA expression levels of hub genes. *** $P<0.05$. Data are presented as the mean \pm SD of at least three repeats. ROS, reactive oxygen species; MDA, malondialdehyde; Fer-1, Ferrostatin-1; ns, not significant; A/R, anoxia/reoxygenation; TEM, transmission electron microscope.

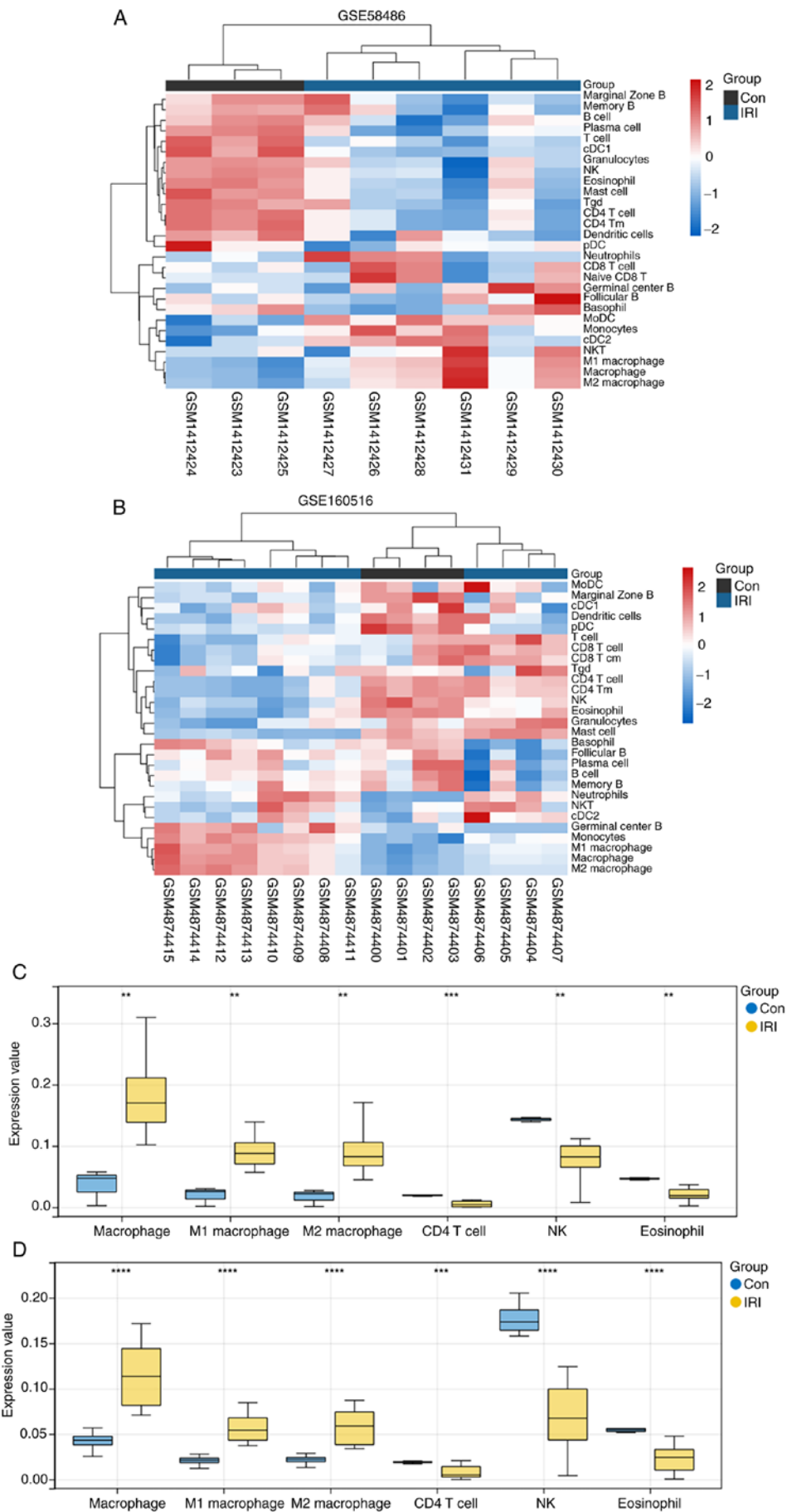


Figure 9. Immune infiltration analyses of the GSE58486 and GSE160516 datasets. Clustering heat map of immune cells in (A) GSE58486 and (B) GSE160516. Differences in the proportion of immune cells in IRI and normal heart samples in (C) GSE58486 and (D) GSE160516. **P<0.01, ***P<0.001, ****P<0.0001. ns, not significant; IRI, ischemia-reperfusion injury.

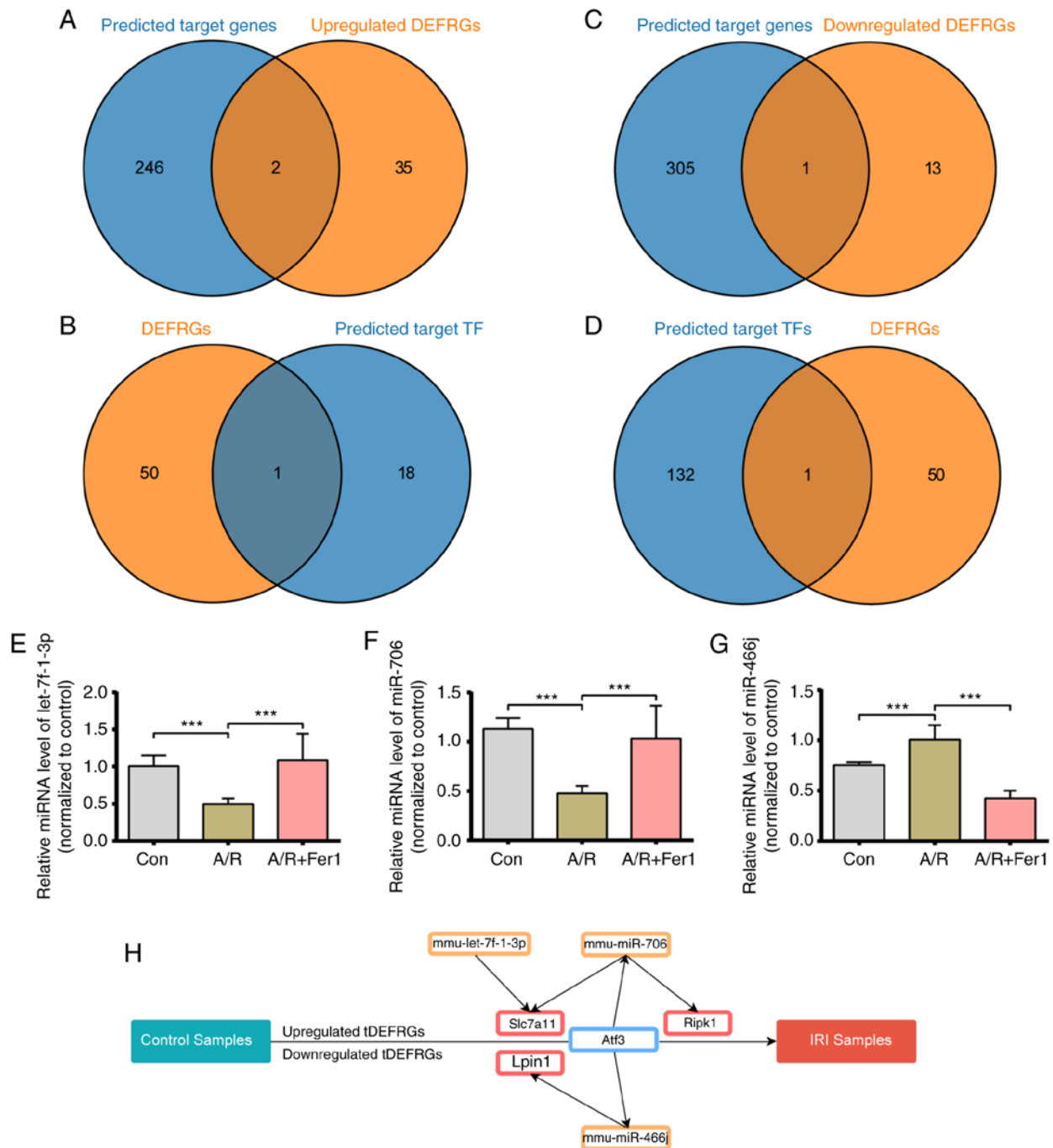


Figure 10. Identified DEmiRs, target genes, and TFs, and construction of DEmiRs-DEFGRs-TFs regulatory network. (A-D) Venn diagram showing the overlap of genes between targeted mRNAs and DEFGRs. (E-G) miRNA expression levels of key miRNAs. (H) DEmiRs-DEFGRs-TF regulatory network. *** $P < 0.05$. Data are presented as the mean \pm SD of at least 3 repeats. TF, transcription factor; DEmiR, differentially expressed microRNA; DEFGR, differentially expressed ferroptosis-related genes; A/R, anoxia/reoxygenation; IRI, ischemia-reperfusion injury.

necessary to identify the connections between ferroptosis and other biological processes in IRI, such as autophagy. Although TGFBI was screened as a hub gene, no changes in its expression levels were found between the control and A/R groups. It is possible that TGFBI mediates ferroptosis during IRI and is altered at the protein level.

As a non-coding RNA, miRNAs can regulate gene expression post-transcriptionally by silencing target mRNAs (52). A TF-miRNA-DEFGR network was established to determine the possible regulatory pathways of the DEFGRs; 3 key miRNAs were identified (mmu-miR-706, mmu-let-7f-1-3p,

and mmu-miR-466j) and were verified experimentally using an *in vitro* A/R model, and the overlapping target DEFGRs and TFs were *SLC7A11*, *RIPK1*, *LIPIN1*, and *ATF3*. Whereas mmu-miR-706 inhibited cardiomyocyte ferroptosis by suppressing *PTGS2* (53), mmu-7f-1-3p alleviated smoke-induced bronchial and alveolar epithelial cell apoptosis via regulating *FOXO1* (54). These potential regulatory pathways may thus offer novel therapeutic targets for the treatment of IRI, and thus warrant further investigation.

Previous studies have demonstrated that the inflammatory response is crucial for the development of IRI, and that any

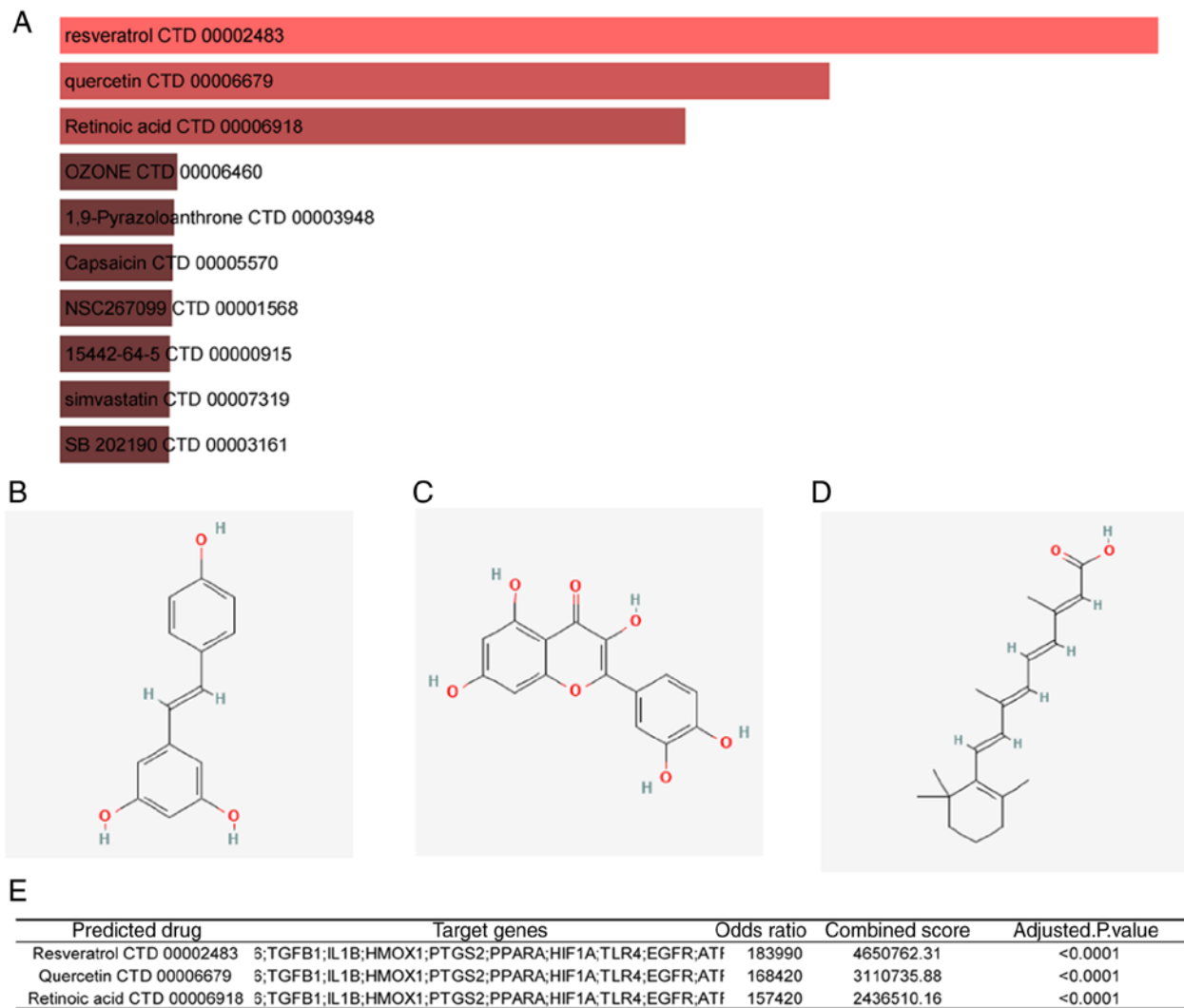


Figure 11. Drugs targeting hub genes. (A) Prediction of drugs that target the hub genes, The top 10 predicted drugs targeting hub genes ranked according to the combined score in the DSigDB database. The chemical structures of (B) resveratrol, (C) Quercetin, (D) retinoic acid. (E) Detailed prediction information of drugs with strong drug-target correlations.

disruption in iron homeostasis affects immune cell function, differentiation and death (55,56). Consistent with this, notable differences in the immune infiltration patterns of normal and IRI samples were observed. While the abundance of M1 and M2 macrophages increased in ischemic heart tissue, that of CD4+ T cells, NK cells, Tregs, eosinophils, and CD4+ Tm cells decreased, consistent with previous studies (57,58). These findings indicate the possibility of crosstalk among the key DEFRGs and aberrant immune responses in IRI, which need to be validated further.

Since the genes involved in pathological processes are potential therapeutic targets (59), the potential drug candidates for the management of IRI based on the ferroptosis-related hub genes were predicted. Resveratrol, quercetin, and retinoic acid showed the highest correlation with the target genes. Retinoic acid was shown to attenuate myocardial injury and inhibit post-IRI cardiomyocyte apoptosis by increasing ADAM10 expression (60). Quercetin exhibited therapeutic effects in different H9c2 cardiomyoblast injury models induced by lipopolysaccharide, doxorubicin, and A/R (61-64). Resveratrol can also protect against IRI by inhibiting ferroptosis and reducing

oxidative stress (65). Nevertheless, further research is needed to determine whether these compounds can alleviate IRI by targeting ferroptosis.

Although the changes in expression levels of hub DEFRGs were validated in another independent dataset, as well as in an *in vitro* experimental model, the exact roles of these genes in the pathological process of IRI requires further clarification using *in vivo* experiments and molecular assays. In addition, although animal models can simulate the morphological signs of human IRI, they cannot recapitulate the natural history and histological features, resulting in potentially inaccurate and even contradictory conclusions. Thus, human tissue samples need to be analyzed to validate our findings. Furthermore, observing the role of the key genes in IRI through more precise interference experiments is critical for the discovery of meaningful therapeutic and diagnostic targets. Therefore, further functional studies are needed to extend the results of the present study to the clinic.

In conclusion, several dysregulated FRGs associated with IRI were identified and experimentally validated, and the aberrant immune infiltration in ischemic heart tissue was explored.

Resveratrol, quercetin, and retinoic acid were also identified as potential candidate drugs for the management of IRI via targeting of ferroptosis. The present study offers novel insight into the role of ferroptosis in IRI, which can help to elucidate its pathobiological mechanisms and identify novel diagnostic and therapeutic targets.

Acknowledgements

Not applicable.

Funding

The present study was supported by the Natural Science Foundation of Jiangxi (grant no. 20212BAB206021), Key Projects of Jiangxi Natural Science Foundation (grant no. 20224ACB206002), the National Natural Science Foundation of China (grant nos. 81860054 and 81960059), and the Major Discipline Academic and Technical Leaders Training Program of Jiangxi Province (grant no. 20204BCJL23056).

Availability of data and materials

The datasets used and/or analyzed during the present study are available from the corresponding author upon reasonable request.

Authors' contributions

SQL, JCL, and HH conceived and designed the study. JCL provided administrative support. SYL, ZHC, FJH, and YCW collected the data. TH, WPY, JCL and HXZ analyzed the data. TH, WPY, and YCW performed the experiments. JCL revised the manuscript. SQL and JCL confirm the authenticity of all the raw data. All authors have read and approved the final manuscript.

Ethics approval and consent to participate

Not applicable.

Patient consent for publication

Not applicable.

Competing interests

The authors declare that they have no competing interests.

References

- Mozaffarian D, Benjamin EJ, Go AS, Arnett DK, Blaha MJ, Cushman M, de Ferranti S, Després JP, Fullerton HJ, Howard VJ, *et al*: Heart disease and stroke statistics-2015 update: A report from the American heart association. *Circulation* 131: e29-e322, 2015.
- O'Gara PT, Kushner FG, Ascheim DD, Casey DE Jr, Chung MK, de Lemos JA, Ettinger SM, Fang JC, Fesmire FM, Franklin BA, *et al*: 2013 ACCF/AHA guideline for the management of ST-elevation myocardial infarction: A report of the American college of cardiology foundation/American heart association task force on practice guidelines. *Circulation* 127: e362-e425, 2013.
- Heusch G and Gersh BJ: The pathophysiology of acute myocardial infarction and strategies of protection beyond reperfusion: A continual challenge. *Eur Heart J* 38: 774-784, 2017.
- Eitel I, Stiermaier T, Rommel KP, Fuernau G, Sandri M, Mangner N, Linke A, Erbs S, Lurz P, Boudriot E, *et al*: Cardioprotection by combined intrahospital remote ischaemic preconditioning and postconditioning in ST-elevation myocardial infarction: The randomized LIPSIA CONDITIONING trial. *Eur Heart J* 36: 3049-3057, 2015.
- Zhou L, Han S, Guo J, Qiu T, Zhou J and Shen L: Ferroptosis-a new dawn in the treatment of organ ischemia-reperfusion injury. *Cells* 11: 3653, 2022.
- Chen X, Li J, Kang R, Klionsky DJ and Tang D: Ferroptosis: Machinery and regulation. *Autophagy* 17: 2054-2081, 2021.
- Tang D, Chen X, Kang R and Kroemer G: Ferroptosis: Molecular mechanisms and health implications. *Cell Res* 31: 107-125, 2021.
- Williams RE, Zweier JL and Flaherty JT: Treatment with deferoxamine during ischemia improves functional and metabolic recovery and reduces reperfusion-induced oxygen radical generation in rabbit hearts. *Circulation* 83: 1006-1014, 1991.
- Paraskevaïdis IA, Iliodromitis EK, Vlahakos D, Tsiapras DP, Nikolaidis A, Marathias A, Michalis A and Kremastinos DT: Deferoxamine infusion during coronary artery bypass grafting ameliorates lipid peroxidation and protects the myocardium against reperfusion injury: Immediate and long-term significance. *Eur Heart J* 26: 263-270, 2005.
- Nakamura T, Naguro I and Ichijo H: Iron homeostasis and iron-regulated ROS in cell death, senescence and human diseases. *Biochim Biophys Acta Gen Subj* 1863: 1398-1409, 2019.
- Ravingerová T, Kindernay L, Barteková M, Ferko M, Adameová A, Zohdi V, Bernátová I, Ferenczyová K and Lazou A: The molecular mechanisms of iron metabolism and its role in cardiac dysfunction and cardioprotection. *Int J Mol Sci* 21: 7889, 2020.
- Edgar R, Domrachev M and Lash AE: Gene expression omnibus: NCBI gene expression and hybridization array data repository. *Nucleic Acids Res* 30: 207-210, 2002.
- Zhou N and Bao J: FerrDb: A manually curated resource for regulators and markers of ferroptosis and ferroptosis-disease associations. *Database (Oxford)* 1: baaa021, 2020.
- Ritchie ME, Phipson B, Wu D, Hu Y, Law CW, Shi W and Smyth GK: limma powers differential expression analyses for RNA-sequencing and microarray studies. *Nucleic Acids Res* 43: e47, 2015.
- R Core Team (2020). R: A language and environment for statistical computing. R Foundation for Statistical Computing, Vienna, Austria. URL <https://www.R-project.org/>.
- Hanbo Chen (2022). VennDiagram: Generate High-Resolution Venn and Euler Plots. R package version 1.7.3. <https://CRAN.R-project.org/package=VennDiagram>
- Huang DW, Sherman BT and Lempicki RA: Systematic and integrative analysis of large gene lists using DAVID bioinformatics resources. *Nat Protoc* 4: 44-57, 2009.
- Huang DW, Sherman BT and Lempicki RA: Bioinformatics enrichment tools: Paths toward the comprehensive functional analysis of large gene lists. *Nucleic Acids Res* 37: 1-13, 2009.
- Ashburner M, Ball CA, Blake JA, Botstein D, Butler H, Cherry JM, Davis AP, Dolinski K, Dwight SS, Eppig JT, *et al*: Gene ontology: Tool for the unification of biology. The gene ontology consortium. *Nat Genet* 25: 25-29, 2000.
- The Gene Ontology Resource: 20 years and still GOing strong. *Nucleic acids research* 47: D330-d338, 2019. doi: 10.1093/nar/gky1055
- Kanehisa M: A database for post-genome analysis. *Trends Genet* 13: 375-376, 1997.
- Szklarczyk D, Gable AL, Lyon D, Junge A, Wyder S, Huerta-Cepas J, Simonovic M, Doncheva NT, Morris JH, Bork P, *et al*: STRING v11: Protein-protein association networks with increased coverage, supporting functional discovery in genome-wide experimental datasets. *Nucleic Acids Res* 47: D607-D613, 2019.
- Shannon P, Markiel A, Ozier O, Baliga NS, Wang JT, Ramage D, Amin N, Schwikowski B and Ideker T: Cytoscape: A software environment for integrated models of biomolecular interaction networks. *Genome Res* 13: 2498-2504, 2003.
- Chin CH, Chen SH, Wu HH, Ho CW, Ko MT and Lin CY: CytoHubba: Identifying hub objects and sub-networks from complex interactome. *BMC Syst Biol* 8 (Suppl 4): S11, 2014.
- Friedman RC, Farh KK, Burge CB and Bartel DP: Most mammalian mRNAs are conserved targets of microRNAs. *Genome Res* 19: 92-105, 2009.

26. Dweep H and Gretz N: MiRWalk2.0: A comprehensive atlas of microRNA-target interactions. *Nat Methods* 12: 697, 2015.
27. Wong N and Wang X: miRDB: An online resource for microRNA target prediction and functional annotations. *Nucleic Acids Res* 43: D146-D152, 2015.
28. Tong Z, Cui Q, Wang J and Zhou Y: TransmiR v2.0: An updated transcription factor-microRNA regulation database. *Nucleic Acids Res* 47: D253-D258, 2019.
29. Huang H, Lai S, Luo Y, Wan Q, Wu Q, Wan L, Qi W and Liu J: Nutritional preconditioning of apigenin alleviates myocardial ischemia/reperfusion injury via the mitochondrial pathway mediated by notch1/hes1. *Oxid Med Cell Longev* 2019: 7973098, 2019.
30. Flameng W, Borgers M, Daenen W and Stalpaert G: Ultrastructural and cytochemical correlates of myocardial protection by cardiac hypothermia in man. *J Thorac Cardiovasc Sur* 79: 413-424, 1980.
31. Livak KJ and Schmittgen TD: Analysis of relative gene expression data using real-time quantitative PCR and the 2(-Delta Delta C(T)) method. *Methods* 25: 402-408, 2001.
32. Miao YR, Zhang Q, Lei Q, Luo M, Xie GY, Wang H and Guo AY: ImmuCellAI: A unique method for comprehensive T-cell subsets abundance prediction and its application in cancer immunotherapy. *Adv Sci (Weinh)* 7: 1902880, 2020.
33. Yoo M, Shin J, Kim J, Ryall KA, Lee K, Lee S, Jeon M, Kang J and Tan AC: DSigDB: Drug signatures database for gene set analysis. *Bioinformatics* 31: 3069-3071, 2015.
34. Li Y, Cao Y, Xiao J, Shang J, Tan Q, Ping F, Huang W, Wu F, Zhang H and Zhang X: Inhibitor of apoptosis-stimulating protein of p53 inhibits ferroptosis and alleviates intestinal ischemia/reperfusion-induced acute lung injury. *Cell Death Differ* 27: 2635-2650, 2020.
35. Lillo-Moya J, Rojas-Solé C, Muñoz-Salamanca D, Panieri E, Saso L and Rodrigo R: Targeting ferroptosis against ischemia/reperfusion cardiac injury. *Antioxidants (Basel)* 10: 667, 2021.
36. Chen X, Kang R, Kroemer G and Tang D: Ferroptosis in infection, inflammation, and immunity. *J Exp Med* 218: e20210518, 2021.
37. Liao P, Wang W, Wang W, Kryczek I, Li X, Bian Y, Sell A, Wei S, Grove S, Johnson JK, *et al*: CD8(+) T cells and fatty acids orchestrate tumor ferroptosis and immunity via ACSL4. *Cancer Cell* 40: 365-378.e6, 2022.
38. Zou HX, Qiu BQ, Lai SQ, Huang H, Zhou XL, Gong CW, Wang LJ, Yuan MM, He AD and Liu JC: Role of ferroptosis-related genes in Stanford type a aortic dissection and identification of key genes: New insights from bioinformatic analysis. *Bioengineered* 12: 9976-9990, 2021.
39. Fang X, Wang H, Han D, Xie E, Yang X, Wei J, Gu S, Gao F, Zhu N, Yin X, *et al*: Ferroptosis as a target for protection against cardiomyopathy. *Proc Natl Acad Sci USA* 116: 2672-2680, 2019.
40. Li W, Feng G, Gauthier JM, Lokshina I, Higashikubo R, Evans S, Liu X, Hassan A, Tanaka S, Cicka M, *et al*: Ferroptotic cell death and TLR4/Trif signaling initiate neutrophil recruitment after heart transplantation. *J Clin Invest* 129: 2293-2304, 2019.
41. Chen Y, Yi X, Huo B, He Y, Guo X, Zhang Z, Zhong X, Feng X, Fang ZM, Zhu XH, *et al*: BRD4770 functions as a novel ferroptosis inhibitor to protect against aortic dissection. *Pharmacol Res* 177: 106122, 2022.
42. Liu X, Bian H, Dou QL, Huang XW, Tao WY, Liu WH, Li N and Zhang WW: Ginkgetin alleviates inflammation, oxidative stress, and apoptosis induced by hypoxia/reoxygenation in H9C2 cells via caspase-3 dependent pathway. *Biomed Res Int* 2020: 1928410, 2020.
43. Bulluck H, Rosmini S, Abdel-Gadir A, White SK, Bhuva AN, Treibel TA, Fontana M, Ramlall M, Hamarneh A, Sirker A, *et al*: Residual myocardial iron following intramyocardial hemorrhage during the convalescent phase of reperfused st-segment-elevation myocardial infarction and adverse left ventricular remodeling. *Circ Cardiovasc Imaging* 9: e004940, 2016.
44. Gao M, Monian P, Quadri N, Ramasamy R and Jiang X: Glutaminolysis and transferrin regulate ferroptosis. *Mol Cell* 59: 298-308, 2015.
45. Wu X, Li Y, Zhang S and Zhou X: Ferroptosis as a novel therapeutic target for cardiovascular disease. *Theranostics* 11: 3052-3059, 2021.
46. Yu Y, Yan Y, Niu F, Wang Y, Chen X, Su G, Liu Y, Zhao X, Qian L, Liu P and Xiong Y: Ferroptosis: A cell death connecting oxidative stress, inflammation and cardiovascular diseases. *Cell Death Discov* 7: 193, 2021.
47. Li Y, Cao Y, Xiao J, Shang J, Tan Q, Ping F, Huang W, Wu F, Zhang H and Zhang X: Inhibitor of apoptosis-stimulating protein of p53 inhibits ferroptosis and alleviates intestinal ischemia/reperfusion-induced acute lung injury. *Cell Death Differ* 27: 2635-2650, 2020.
48. Liu S, Yan S, Zhu J, Lu R, Kang C, Tang K, Zeng J, Ding M, Guo Z, Lai X, *et al*: Combination RSL3 treatment sensitizes ferroptosis- and EGFR-inhibition-resistant HNSCCs to cetuximab. *Int J Mol Sci* 23: 9014, 2022.
49. Meng Z, Liang H, Zhao J, Gao J, Liu C, Ma X, Liu J, Liang B, Jiao X, Cao J and Wang Y: HMOX1 upregulation promotes ferroptosis in diabetic atherosclerosis. *Life Sci* 284: 119935, 2021.
50. Wang L, Liu Y, Du T, Yang H, Lei L, Guo M, Ding HF, Zhang J, Wang H, Chen X and Yan C: ATF3 promotes erastin-induced ferroptosis by suppressing system Xc. *Cell Death Differ* 27: 662-675, 2020.
51. Liu T, Shu J, Liu Y, Xie J, Li T, Li H and Li L: Atorvastatin attenuates ferroptosis-dependent myocardial injury and inflammation following coronary microembolization via the Hif1a/Ptgs2 pathway. *Front Pharmacol* 13: 1057583, 2022.
52. Liu H, Mo H, Yang C, Mei X, Song X, Lu W, Xiao H, Yan J, Wang X, Yan J, *et al*: A novel function of ATF3 in suppression of ferroptosis in mouse heart suffered ischemia/reperfusion. *Free Radic Biol Med* 189: 122-135, 2022.
53. van Wijk N, Zohar K and Linial M: Challenging cellular homeostasis: Spatial and temporal regulation of miRNAs. *Int J Mol Sci* 23: 16152, 2022.
54. Gao F, Zhao Y, Zhang B, Xiao C, Sun Z, Gao Y and Dou X: Suppression of lncRNA Gm47283 attenuates myocardial infarction via miR-706/Ptgs2/ferroptosis axis. *Bioengineered* 13: 10786-10802, 2022.
55. Han Z, Zhu Y, Cui Z, Guo P, Wei A and Meng Q: MicroRNA Let-7f-1-3p attenuates smoke-induced apoptosis in bronchial and alveolar epithelial cells in vitro by targeting FOXO1. *Eur J Pharmacol* 862: 172531, 2019.
56. Bacmeister L, Schwarzl M, Warnke S, Stoffers B, Blankenberg S, Westermann D and Lindner D: Inflammation and fibrosis in murine models of heart failure. *Basic Res Cardiol* 114: 19, 2019.
57. Ni S, Yuan Y, Kuang Y and Li X: Iron metabolism and immune regulation. *Front Immunol* 13: 816282, 2022.
58. Fan Q, Tao R, Zhang H, Xie H, Lu L, Wang T, Su M, Hu J, Zhang Q, Chen Q, *et al*: Dectin-1 contributes to myocardial ischemia/reperfusion injury by regulating macrophage polarization and neutrophil infiltration. *Circulation* 139: 663-678, 2019.
59. Sun K, Li YY and Jin J: A double-edged sword of immunomicroenvironment in cardiac homeostasis and injury repair. *Signal Transduct Target Ther* 6: 79, 2021.
60. Huang M, Cai S and Su J: The pathogenesis of sepsis and potential therapeutic targets. *Int J Mol Sci* 20: 5376, 2019.
61. Zhu Z, Zhu J, Zhao X, Yang K, Lu L, Zhang F, Shen W and Zhang R: All-trans retinoic acid ameliorates myocardial ischemia/reperfusion injury by reducing cardiomyocyte apoptosis. *PLoS One* 10: e0133414, 2015.
62. Li C, Zhang WJ and Frei B: Quercetin inhibits LPS-induced adhesion molecule expression and oxidant production in human aortic endothelial cells by p38-mediated Nrf2 activation and antioxidant enzyme induction. *Redox Biol* 9: 104-113, 2016.
63. Chen X, Peng X, Luo Y, You J, Yin D, Xu Q, He H and He M: Quercetin protects cardiomyocytes against doxorubicin-induced toxicity by suppressing oxidative stress and improving mitochondrial function via 14-3-3γ. *Toxicol Mech Methods* 29: 344-354, 2019.
64. Tang L, Peng Y, Xu T, Yi X, Liu Y, Luo Y, Yin D and He M: The effects of quercetin protect cardiomyocytes from A/R injury is related to its capability to increasing expression and activity of PKCε protein. *Mol Cell Biochem* 382: 145-152, 2013.
65. Li T, Tan Y, Ouyang S, He J and Liu L: Resveratrol protects against myocardial ischemia-reperfusion injury via attenuating ferroptosis. *Gene* 808: 145968, 2022.

